

Wang, F., Lühr, H., Xiong, C., Park, J., Zhou, Y.  
(2023): Global Characteristics of Improved  
Interhemispheric Field-Aligned Currents and of F-  
Region Meridional Currents Observed by the  
Swarm Dual-Spacecraft. - Journal of Geophysical  
Research: Space Physics, 128, 2, e2022JA031096.

<https://doi.org/10.1029/2022JA031096>

# JGR Space Physics

## RESEARCH ARTICLE

10.1029/2022JA031096

### Key Points:

- The tidal activity at mid-latitudes is better organized in UT than in MLT, with the strongest IHFAC appearing around 18–19 UT
- The IHFAC density around noon reduces remarkably poleward of 37 magnetic latitudes in summer and even reverse the direction during winter
- The FMC are highly symmetric with respect to the magnetic equator and quite weak, amounting only to one-third or half of the IHFAC density

### Correspondence to:

C. Xiong,  
[xiongchao@whu.edu.cn](mailto:xiongchao@whu.edu.cn)

### Citation:






Wang, F., Lühr, H., Xiong, C., Park, J., & Zhou, Y. (2023). Global characteristics of improved interhemispheric field-aligned currents and of F-region meridional currents observed by the Swarm dual-spacecraft. *Journal of Geophysical Research: Space Physics*, 128, e2022JA031096. <https://doi.org/10.1029/2022JA031096>

Received 19 OCT 2022

Accepted 26 JAN 2023

© 2023. American Geophysical Union.  
All Rights Reserved.

## Global Characteristics of Improved Interhemispheric Field-Aligned Currents and of F-Region Meridional Currents Observed by the Swarm Dual-Spacecraft

Fengjue Wang<sup>1</sup> , Hermann Lühr<sup>2</sup> , Chao Xiong<sup>1,3</sup> , Jaeheung Park<sup>4,5</sup> , and Yunliang Zhou<sup>1</sup> 

<sup>1</sup>Department of Space Physics, School of Electronic Information, Wuhan University, Wuhan, China, <sup>2</sup>GFZ German Research Centre for Geosciences, Section 2.3, Geomagnetism, Telegrafenberg, Potsdam, Germany, <sup>3</sup>Hubei LuoJia Laboratory, Wuhan, China, <sup>4</sup>Space Science Division, Korea Astronomy and Space Science Institute (KASI), Daejeon, South Korea, <sup>5</sup>Department of Astronomy and Space Science, University of Science and Technology (UST), Daejeon, South Korea

**Abstract** The Swarm satellite constellation provides an excellent opportunity to explore ionospheric current systems. In this study, we have reanalyzed the ionospheric currents derived by the Swarm dual-satellite approach, to investigate the characteristic of inter-hemispheric field-aligned currents (IHFAC). One major improvement is that the influence of the ambient magnetic field on the IHFAC intensity has been taken into account, and the derived IHFAC densities are normalized to their ionospheric E-region footprints. In addition, we have extended the analysis to the middle latitudes within  $\pm 60^\circ$  MLat, which show IHFAC features different from those at low latitudes. For the first time the tidal features at mid-latitudes are studied. They are dominated by longitudinal wave-1 and wave-2 patterns. A superposition of these tidal components reflects a confinement of the IHFAC tidal modulation to daytime in the western hemisphere. The tidal signatures at middle latitudes are better organized in universal time than in local time. The strongest IHFACs are appearing around 18–19 UT, near noon in the American sector. This is related to the overlap with the South Atlantic Anomaly. For the first time we define and analyze the F-region meridional currents (FMC), interpreting the remaining part of the ionospheric radial current (IRC), which is not covered by IHFAC. The mean FMCs are found to be highly symmetric with respect to the magnetic equator and only amounts to one-third or half of the IHFAC density, however, they show neither typical longitudinal, diurnal variations, or tidal signatures.

## 1. Introduction

The solar quiet daily variation (Sq) currents are known to cause prominent magnetic field variations at low and middle latitudes (Campbell, 1989). These currents in the dayside ionospheric E-layer flows clockwise in the southern hemisphere and counter-clockwise in the northern hemisphere, with vortices centered at about  $\pm 35^\circ$  magnetic latitude (MLat). As the atmospheric wind and ionospheric conductivity depend on the intensity of solar extreme ultraviolet (EUV) radiation, ionospheric currents show prominent seasonal dependence. Compared to equinoxes, the summer hemispheric atmosphere during solstice is more effectively ionized and with that the hemispheric difference in ionospheric current intensity is larger (Van Sabben, 1964). As a consequence, inter-hemisphere field-aligned currents (IHFAC) were predicted to flow from one hemisphere to the other, connecting the vortices of the Sq current systems in order to balance the potential differences between the two hemispheres (Fukushima, 1979).

Earlier studies used mainly the magnetic signatures from ground magnetometers (Forbes, 1981; Rastogi, 1989), or sounding rocket (e.g., Onwumechili, 1992), to investigate the characteristics of ionospheric currents. However, Fukushima et al. (1976) pointed out that the magnetic signatures from ground magnetometers cannot effectively distinguish contributions from the magnetospheric and ionospheric currents. Therefore, in situ magnetic measurements from low-Earth orbit (LEO) satellites became an important data source for resolving these currents (e.g., Cain & Sweeney, 1973; Langel et al., 1993; Lühr et al., 2004), as all LEO satellites fly above the E-region current but below the magnetospheric current, for example, the ring current. Compared to ground magnetometer and rocket, LEO satellites pass very rapidly over the ionospheric current system and their measurements thus can be regarded as a snapshot of the spatial structures. The F-region currents during daytime are much weaker compared to the E-region current, for example, Sq currents or equatorial electrojet (EEJ), therefore, magnetic field measurements with high resolution are required to resolve the F-region currents.

One good example is the high-resolution magnetic measurements from the Challenging Mini-satellite Payload (CHAMP) satellite, which provided the first direct evidence of the daytime F region dynamo-driven currents flowing downward around noon and upward around dusk at the dip equator (Lühr & Maus, 2006). In addition, magnetic measurements from CHAMP and later Swarm missions have been used for resolving the dependence of IHFACs on solar activity and longitude (Park et al., 2011; Lühr et al., 2015). They found that the longitudinal distribution of IHFAC shows remarkable seasonal difference. For example, the mean IHFAC exhibits four intensity peaks during equinoxes and June solstice, which is known from earlier studies as the longitudinal wave-4 pattern and is attributed mainly to the diurnal non-migrating solar tidal component DE3 (e.g., Immel et al., 2006; Lühr & Manoj, 2013), while the IHFAC in December solstice is dominated by the semidiurnal westward propagating solar tide SW1 (Lühr et al., 2019).

Though several studies have been performed focusing on the features of IHFAC, there are still open questions that need to be further addressed. One issue is the seasonal dependence and flow direction of IHFAC. From theoretical prediction, IHFAC is expected to be larger in solstice seasons than during equinoxes. However, observations from CHAMP and Swarm showed that the intensity of IHFACs during autumn equinox is closer to the values around June solstice, but much larger than the values in December solstice (e.g., Lühr et al., 2019; Park et al., 2011). In addition, Fukushima (1979) predicted that the IHFACs flow from the summer to winter hemisphere at both noon and dusk hours. Such a flow pattern from summer to winter hemisphere has been confirmed from CHAMP and Swarm observations only at noon, while at dusk an opposite direction flow has been observed (e.g., Lühr et al., 2015; Park et al., 2011). The second issue is the proper deduction of IHFAC from satellite magnetic measurements. IHFACs, or field-aligned currents (FACs) are mostly derived from single satellite missions, while for the Swarm mission, consisting of three satellites, these currents can also be obtained from the dual-spacecraft (dual-SC) approach, by taking advantage of the Swarm A and C satellites flying in a side-by-side configuration (Lühr et al., 2020; Ritter et al., 2013). This latter approach makes use of Ampère's integral law applied to a quad formed by four B-field measurements from the two satellites. Wang et al. (2022) confirmed that the dual-SC approach can yield more reliably the ionospheric radial current (IRC) component and FAC, with improvements both in current intensity and distribution.

In addition, so far most of the studies considered only the low-latitude parts of IHFACs and IRCs, not exceeding 40° MLat. Just Fathy et al. (2019) examined the FAC distribution derived from Swarm over the MLat ranges between 15° and 55° MLat in both hemispheres. However, they didn't provide any interpretation of the current distribution that they presented. Park et al. (2020) were the first to identify a kind of demarcation line around  $\pm 35^\circ$  MLat when looking at the radial currents, IRC, from Swarm over the  $\pm 60^\circ$  MLat range. Near this line the character of IRC changes significantly, with largely reversed sign of flow polarity. Their interpretation, aided by TIME-GCM simulations, suggest solar tidal forcing as the prime source for the observed current direction reversal. As a caveat, it may be mentioned that the authors interpreted only the radial current component. But, from the perspective of ionospheric physics, the radial current has in general no particular relevance. It is more appropriate to describe currents in their three principal components: field-aligned, and the two transverse components. Furthermore, the less reliable IRC estimates from single-satellite had been used in their study.

Our aim of this study is to provide a highly reliable presentation of the mean IHFAC distribution at low and middle latitudes, separately for the seasons and different local time sectors. Their climatological characteristics will be derived from the Swarm data of the years 2014–2019. Besides the IHFAC, estimates of the meridional transverse currents will also be shown for the first time. These F-region currents are expected to be mainly driven by thermospheric zonal winds.

In the sections to follow we first introduce the data considered and equations for calculating the current components from the prime IRC current product. Section 3 presents first the various IHFAC distributions derived from Swarm observations and then the mean meridional currents. Subsequently, in Section 4 obtained results are discussed and compared with previous studies. Toward the end of the section, we focus on the tidal features of the IHFACs separately for low- and mid-latitude parts. Finally, there will be a Summary and Conclusion rounding up the study.

## 2. Data and Processing Approaches

### 2.1. Swarm Satellites and Ionospheric Current Products

ESA's Swarm mission was launched on 22 November 2013. It consists of three identical satellites in near-polar orbits at different altitudes. During the first mission phase, starting in 17 April 2014, the lower pair, Swarm A and C, were flying side-by-side with a longitudinal separation of  $1.4^\circ$ , while third one, Swarm B, cruised about 50 km higher. The second mission phase started in October 2019. In preparation for the counter-rotation campaign the separation between Swarm A and C was then slowly reduced. Due to their orbital precession, Swarm A/C needs about 133 days to cover the 24-hr local time (LT), while Swarm B needs about 141 days (e.g., Xiong et al., 2018).

In this study, we used the 1 Hz Level-1b magnetic field data with product identifier "MAGx\_LR" and the 1 Hz Level-2 FAC data with product identifier "FACx\_TMS." The small "x" in the product names represents a placeholder for the spacecraft names, A, B, C. Of particular interest for this work are IRC and FAC estimates both derived from the combined magnetic field measurements of Swarm A and C. These results exhibit clear advantages over the corresponding estimates from single satellites, as has been shown by Wang et al. (2022). Methods and assumptions on how the FAC and IRC are calculated from the magnetic measurements of single satellite and dual spacecraft have been described by Lühr et al. (2020).

An important prerequisite for reliable dual-SC current estimates is a highly precise calibration of the vector magnetometers on the Swarm A and C spacecraft. However, during certain local times, as has been shown by Wang et al. (2022), there were obvious deficits, in particular around sunrise. We want to note that the Swarm magnetic and IRC/FAC products have recently been updated. To illustrate the difference between old data (version 03) and updated ones (version 04), Figure 1 shows two examples of IRC and FAC latitude profiles for 1 May 2014 (top) and 13 April 2019 (bottom). Both these examples had earlier been presented in Figure 2 of Wang et al. (2022). The black curves show the currents derived from the old data, and the red are based the latest data. We can see, for the first example, from 1 May 2014, the updated IRC and FAC reproduce very well the old ones with only very minor difference at some points. While in the second example, from 13 April 2019, the IRC and FAC show significant differences between the old and new data versions. The latest IRC and FAC curves fluctuate around zero, as expected, while the old ones exhibit a bias of about  $10 \text{ nA m}^{-2}$ . Note that Swarm orbited around 5.68 magnetic local time (MLT) and the low-latitude FACs at this early morning should be quite weak, as confirmed by the advanced data. The comparison shown here indicates that the updated IRC and FAC data are more reliable. However, by a systematic survey based on the 5-year data period of version 04, this spurious morning signature partly remains in the average values of descending orbits, as was the case in data of version 03 (see Figure 6 of Wang et al., 2022). Since the hours around 04:00–06:00 MLT are not of main concern for our current study and the mean bias ranges only around  $2 \text{ nA/m}^2$ , we do not think this effect is influencing our main results.

### 2.2. Estimation of Ionospheric Currents

One of the advanced Swarm data products is the IRC, which is derived from the magnetic measurements of Swarm A and C, flying in close constellation. By applying Ampère's law in integral form, the result represents only the mean current density of the radial component flowing through the contour, framed by the B-field measurements at the four corners of a quad. For more details of the approach see Ritter et al. (2013) and Lühr et al. (2020). Magnetic effects of remote current systems, for example, electrojets, ring current, or Sq current, which can be represented by a scalar potential, make no contributions to the IRCs. Scalar potentials do not contribute to a closed-loop integration. It has to be noted that due to the averaging over the integration quad only large-scale vertical current features with sizes more than 150 km (dimension of the quad) can be resolved.

As mentioned above, from the geophysical point of view it is appropriate to describe the ionospheric currents in their three principal components, the field-aligned and the two transverse. From the latter two components, one is chosen perpendicular to the B field and within the magnetic meridional plane, while the remaining one is the horizontal zonal current, which is perpendicular to the radial direction. We are thus left with the task to separate the FAC contribution within the IRC results from the meridional perpendicular current part. For accomplishing that certain assumptions have to be made:

1. Due to the high conductivity along magnetic field lines, the FACs are expected to be most significant. For deriving the full FAC intensity we map the IRC value onto the field direction by making use of the local magnetic inclination angle.

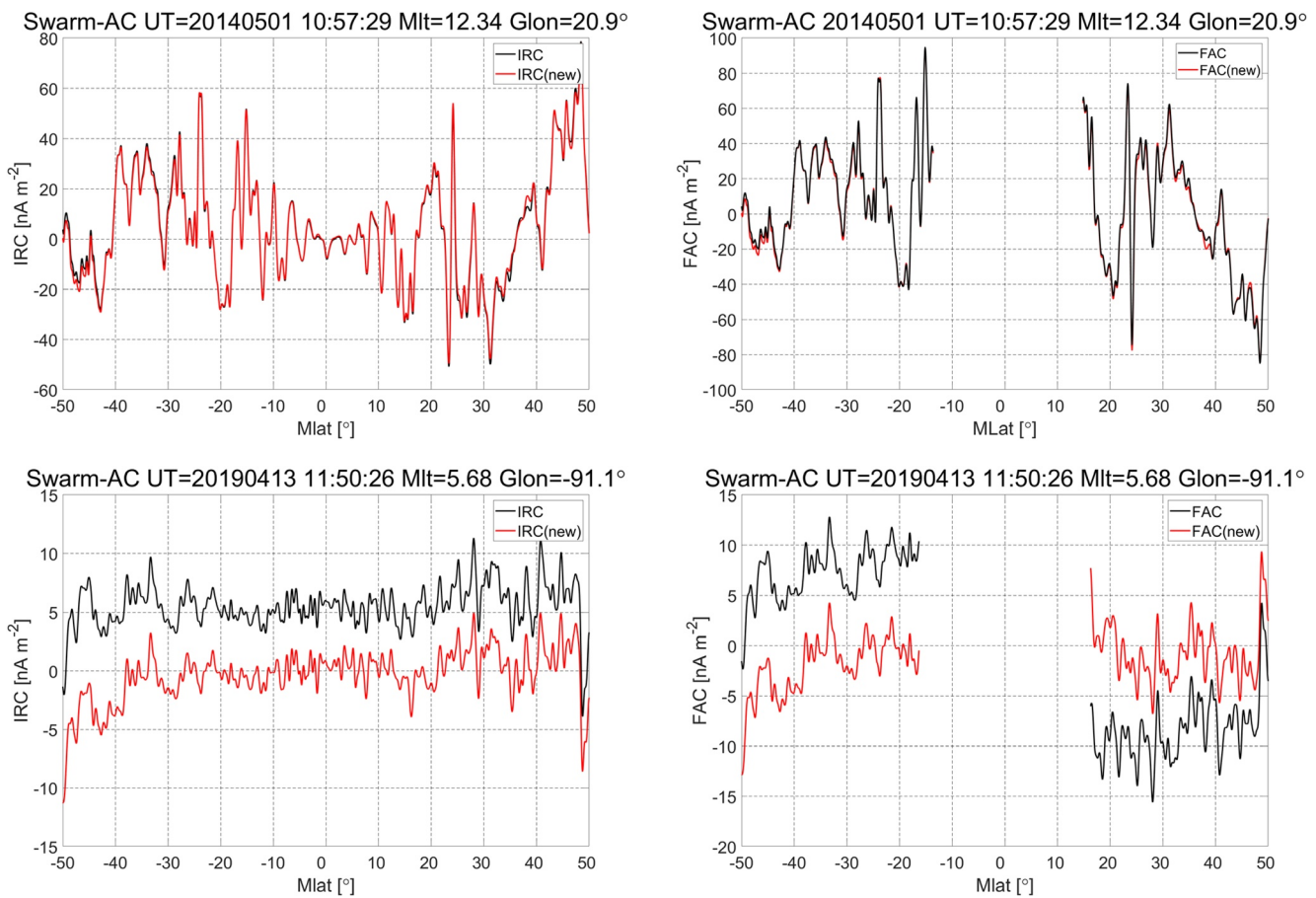


**Figure 1.** Two examples of ionospheric radial currents (IRC) and field-aligned current (FAC) density profiles over geomagnetic latitude. Black curves represent results based on the old data version (earlier presented in Figures 2 and 3 of Wang et al. (2022), for these two orbits). The red curves show the current profiles based on the latest version 04. Current densities in the top row, from 1 May 2014 around noon, show no differences between the two versions. Conversely in the bottom row, from 13 April 2019 at early morning, the current profiles based on the old data (black curves) are clearly offset from near-zero level.

2. Requiring current continuity of FACs. The same amount of current has to be found at conjugate locations in the two hemispheres. This common current component is called IHFAC, flowing from south to north for a positive sign.
3. The remaining anti-symmetric part of radial currents, at conjugate locations, is interpreted as F region meridional current (FMC), and it is mapped onto the direction perpendicular to the  $B$ -field with the help of the local inclination.

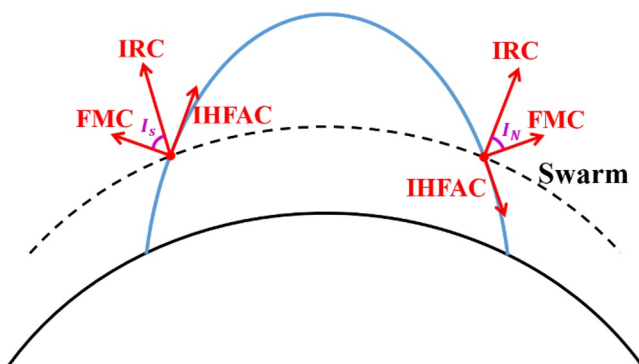


**Figure 2.** Sketch of local current vectors in the field-aligned frame. All the arrows point into the positive current directions. The blue line represents a magnetic field line, while the black dashed line indicates the track of Swarm.

A sketch illustrating the relation between IHFAC, FMC, and IRC in the two hemispheres is shown in Figure 2. All the vector point into their positive directions in both hemispheres.

### 2.2.1. Calculation of IHFAC

We start from the calculation of FAC that is derived from IRC by mapping the vertical current component onto the ambient magnetic field direction by means of the magnetic declination angle,  $I$ . Note that the inclination is positive in the northern and negative in the southern hemisphere. The current flow direction is thus defined positive from the southern to the northern hemisphere along the  $B$ -field.

$$\text{FAC} = \frac{\text{IRC}}{-\sin I} \quad (1)$$

For IHFAC, it is requested that a constant amount of current flows along a magnetic fluxtube, which can be represented to first order by the average FAC density from conjugate points:

$$\text{IHFAC}_O = \frac{(\text{FAC}_N + \text{FAC}_S)}{2} \quad (2)$$

where  $\text{FAC}_N$ ,  $\text{FAC}_S$  are FAC density readings in the northern and southern hemisphere, respectively. However, the FAC density within a fluxtube varies with the ambient field strength. In stronger field regions the currents are denser. Generally, there can be significant differences between the geomagnetic field at conjugate points in the northern and southern hemispheres. Partly, the magnetic flux density at conjugate points differs at middle latitudes up to a factor of 2. For taking these asymmetries into account, the local FAC readings have to be normalized by the ambient field strength. Another shortcoming of Equation (2) is that the derived  $\text{IHFAC}_O$  is valid only at the actual satellite altitude. But the Swarm A and C altitudes gradually decrease from 460 to 410 km during the considered 5 years. This will affect the derived IHFAC values. Therefore, another modification is applied to Equation (2), the IHFAC values are normalized to the footprint of the field line in the E-region, as reference altitude. For that the considered field line is traced down to the ionosphere, and the current density is scaled up by the field strength at that point. The final equations for the IHFAC values in the two hemispheres are:

$$\text{IHFAC}_N = -\frac{1}{2} \left( \frac{\text{IRC}_S}{B_{F,S} \sin I_S} + \frac{\text{IRC}_N}{B_{F,N} \sin I_N} \right) B_{\text{ion},N} \quad (3)$$

$$\text{IHFAC}_S = -\frac{1}{2} \left( \frac{\text{IRC}_S}{B_{F,S} \sin I_S} + \frac{\text{IRC}_N}{B_{F,N} \sin I_N} \right) B_{\text{ion},S} \quad (4)$$

where  $B_{F,N}$  and  $B_{F,S}$  are the magnetic field strength at conjugate latitudes along the satellite orbit in the northern and southern hemispheres, respectively,  $B_{\text{ion},N}$  and  $B_{\text{ion},S}$  are the northern and southern magnetic field intensities at the ionospheric field line footprints (at 110 km) in the two hemispheres, respectively. Having the IHFAC densities normalized to the ionosphere footprints makes the results independent of measurement height.

### 2.2.2. Calculation of FMC

The remaining part of IRC, after evaluating the IHFACs, is interpreted as meridional transverse current. At a local position, for example, in the northern hemisphere, the split of IRC can be described as follows:

$$\text{IRC}_N = \text{FMC}_N \cdot \cos I_N - \text{IHFAC}_N \cdot \frac{B_{F,N} \cdot \sin I_N}{B_{\text{ion},N}} \quad (5)$$

By solving the above formula for FMC density estimates, the equations for the two hemispheres are:

$$\text{FMC}_N = \left( \text{IRC}_N - \text{IRC}_S \frac{B_{F,N} \cdot \sin I_N}{B_{F,S} \cdot \sin I_S} \right) / 2 \cos I_N \quad (6)$$

$$\text{FMC}_S = \left( \text{IRC}_S - \text{IRC}_N \frac{B_{F,S} \cdot \sin I_S}{B_{F,N} \cdot \sin I_N} \right) / 2 \cos I_S \quad (7)$$

The subscripts  $N$  and  $S$  represent again northern and southern hemispheres, respectively. The FMC is almost identical with IRC near the magnetic equator due to the small inclination angle there. We want to note that the FMC reflects the local current density at the actual satellite altitude (460–410 km), different to our IHFACs that are normalized to the ionospheric footprint altitude. We see no simple way of normalizing FMC to a reference altitude.

## 3. Results

In this study we focus on the climatological features of the ionospheric currents at low and middle latitudes. Therefore, averages over 5 years are considered. This time period guarantees an even coverage of local times over all seasons by the Swarm satellites. It avoids possible biases that may appear when taking shorter intervals. The data from 17 April 2014 (start of the dedicated constellation) to 16 April 2019 are used. During this time the solar activity varied from moderately high to low level, with F10.7 decreasing from about 150 to 70 sfu. Also, the magnetic activity was generally moderate to low, except for a few magnetic storms.

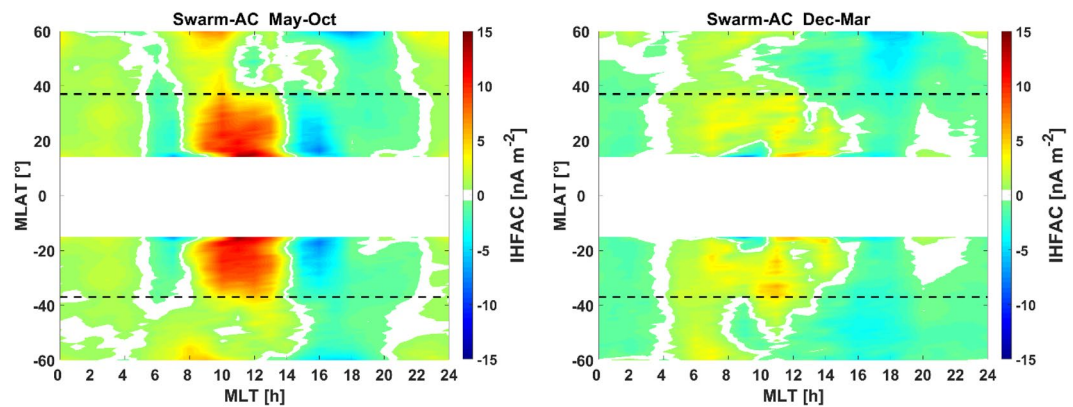


**Figure 3.** Magnetic latitude versus magnetic local time distributions of the IHFAC using the modified formula derived from new data set, separately for (left) summer and (right) winter seasons. The dashed lines represent  $\pm 37^\circ$  MLat.

In the following we are first presenting the mean properties of the newly processed IHFACs. These cover the magnetic latitude range from  $15^\circ$  to  $60^\circ$  MLat in both hemispheres. The lower boundary is due to a consequence of the decreasing angle between orbit track and the magnetic field lines toward lower latitudes, which makes the estimates of FAC increasingly difficult. The limit of  $15^\circ$  has been chosen as a viable compromise between good coverage and increasing uncertainty (e.g., Ritter et al., 2013).

### 3.1. Mean Properties of the IHFAC

As mentioned, most earlier studies that made use of the Swarm dual-SC FAC estimates, for example, Lühr et al. (2019) and Wang et al. (2022), were limited to magnetic latitudes below about  $\pm 40^\circ$  MLat. Park et al. (2020) were the first to note that the characteristics of IHFACs change significantly at a demarcation line running approximately along  $\pm 35^\circ$  MLat. That means, the mid-latitude part of IHFACs, poleward of  $35^\circ$  MLat, has not been investigated in sufficient depth. For that reason, our study will focus mainly on this higher latitude zone, and we will make repeatedly references to earlier works when describing the low-latitude IHFACs.

At first, we take a look at the average flow direction change of IHFAC. Figure 3 shows the mean local time variation (averaged over all longitudes) of IHFAC separately for two prime seasons. It had already been noted by Park et al. (2011) that the IHFAC characteristics do not follow well the standard seasonal patterns. Rather, June solstice and autumn equinox patterns are quite similar, while markedly different features appear during the months from December to March. We follow this division and term conveniently in the following the period from May to October as “summer,” and from December to March as “winter.”

In the left frame of Figure 3, for summer, the typical current patterns appear at low latitudes, with intense IHFACs from the southern to the northern hemisphere around noon and weaker currents in the opposite direction during morning and evening hours. IHFACs practically vanish during nighttime. This has been reported many times before, for example, Park et al. (2011, 2020) and Lühr et al. (2015, 2019). Dashed lines are added at  $\pm 37^\circ$  MLat, which corresponds to the  $\pm 35^\circ$  MLat of Park et al. (2020), by taking into account our field-aligned mapping from satellite height to E-region altitude. Poleward of the  $37^\circ$  demarcation lines, the mean current densities during daytime are markedly lower, but not much changes in flow direction. Conversely, during our winter as shown in the right frame of Figure 3, no such clear mean local time pattern emerges. In the low-latitude zone northward IHFACs are prevailing from the morning to afternoon hours, although at low intensity. Only in the evening we see weak southward currents. Also here, we find some characteristic changes at the demarcation line, but everything shows quite low current density. All the local time characteristics presented here are comparable with the features presented by Park et al. (2020), as shown in their Figures 3d–3f. Qualitatively, the results agree with each other, but their reported current densities are much lower because they considered only IRCs from single-satellite solutions.

The mean local time variation provides only limited information about the actual current distribution. Therefore, we have plotted in Figure 4 the whole IHFAC distribution in latitude (GLat) versus geographic longitude (GLon) frames separately for the noon, morning, and evening time sectors. When starting with the summer-time noon

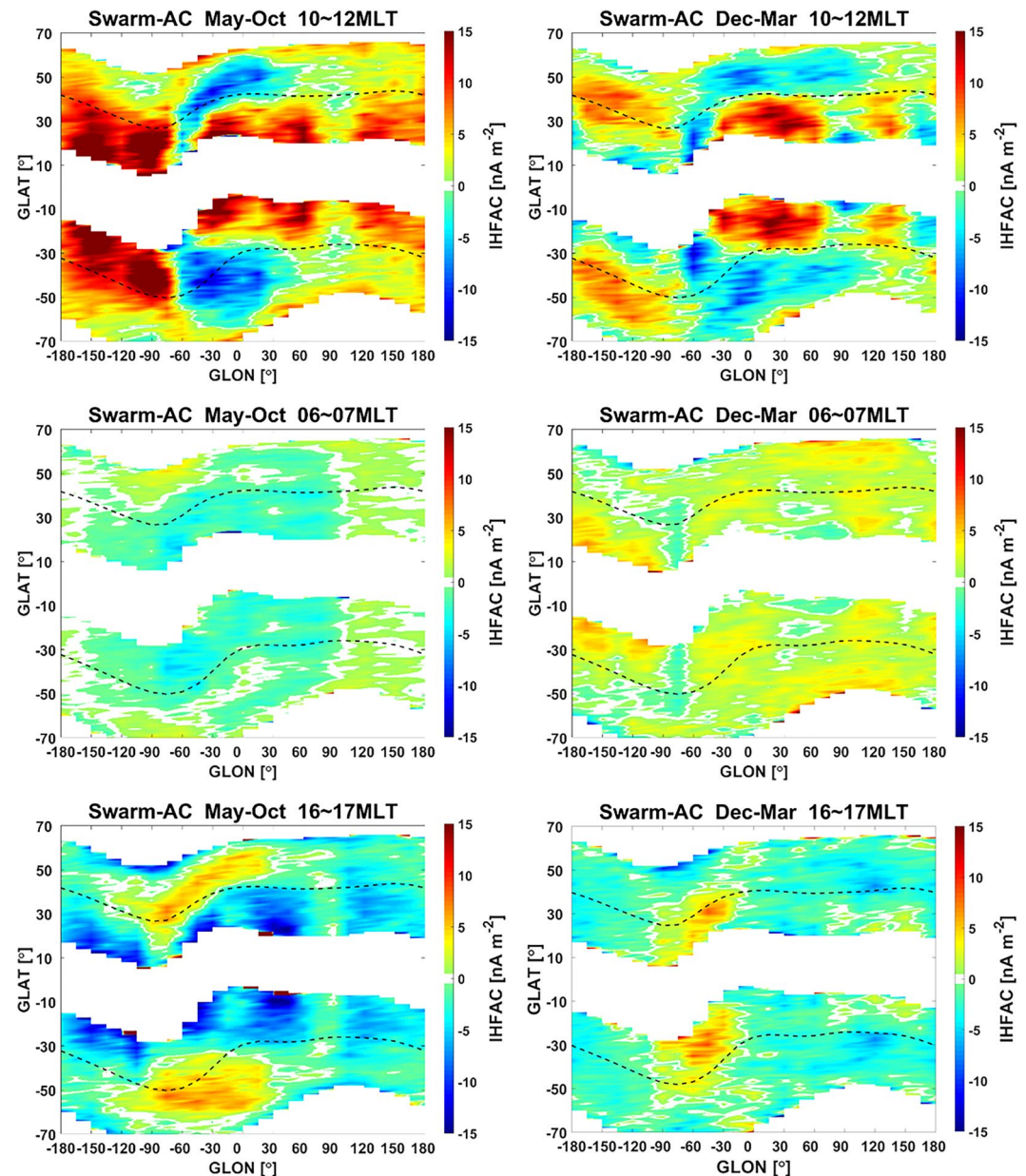


**Figure 4.** Geographic latitude versus longitude distribution of IHFAC from new data set of Swarm AC during summer and winter season, separately for (top) 10~12 MLT (middle) 06~07 MLT, and (bottom) 16~17 MLT. Blacked dashed lines denote  $\pm 37^\circ$  MLat.

sector, the intense low-latitude northward currents show a clear longitudinal structure, which has earlier been related to a wave-4 pattern associated with the diurnal solar tide, DE3, for example, Park et al. (2011), Lühr et al. (2019), and Wang et al. (2022). Only around the longitudes of the South Atlantic Anomaly (SAA) this pattern is somewhat disturbed. Conversely, in the mid-latitude zone, beyond the  $37^\circ$ -line, there are no wave-4 patterns discernible. During the winter period, around noontime, the IHFAC directions and intensities vary more over longitude. This is the reason for the rather weak mean diurnal variation current density. Over the Eurasian longitude sector ( $30^\circ\text{W}$ – $90^\circ\text{E}$ ) we find intense northward IHFACs at low latitudes and currents in the opposite direction at mid latitudes. Just the reversed current flow situation is prevailing over the eastern Pacific ( $90^\circ\text{W}$ – $180^\circ\text{W}$ ); intense northward currents at mid latitudes and weaker southward at low latitudes.

When looking at morning hours, the differences of IHFAC distribution between mid and low latitudes largely disappear. More obvious are the changes with longitude. During our summer the current direction changes,



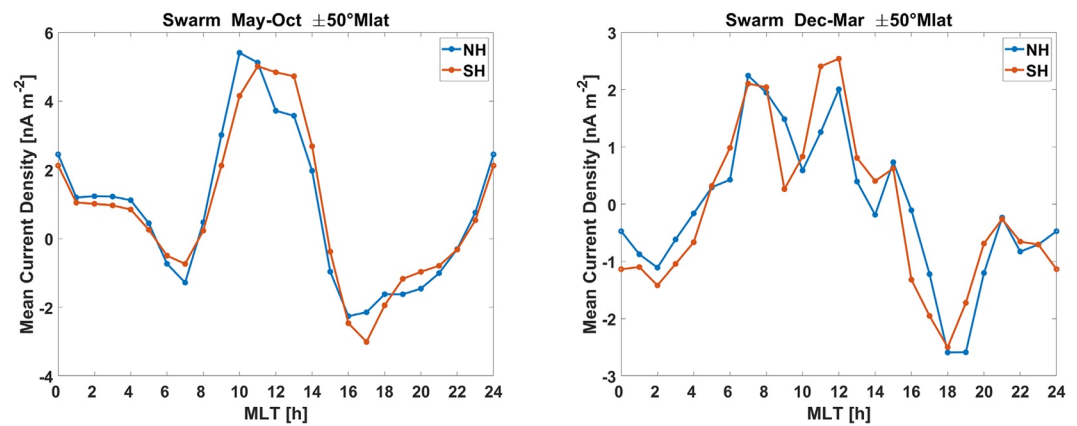


**Figure 5.** Comparison of mean current density in the northern and southern hemisphere.

although at low density, within 115°E–180°E from southward to northward. Only around the SAA longitude (~60°W) northward currents at mid latitude are paired with southward currents at low latitude. During winter the IHFAC direction is predominantly northward, and in the sector over the eastern Pacific (90°W–180°W), westward of the SAA, the distribution changes to northward at low and southward currents at mid latitudes.

Around the evening sector southward IHFACs are dominating in both our seasons. During summer the wave-4 longitudinal pattern is again quite obvious at low latitudes. Conversely, at middle latitudes there appears prominent northward current in the longitude sector 90°W–30°E. In winter months the IHFAC distribution shows in general little longitudinal structure. An exception makes the longitude region around the SAA. Here we find significant northward IHFACs at low latitudes surrounded by a generally southward environment. This means, only in the vicinity of the SAA the current flow directions in the two latitude zones switch between our two periods. Generally, we may conclude that the longitudinal averaged local time variations, as shown in Figure 3, do not represent the diurnal dynamics of the IHFACs too well.

When comparing the IHFAC distributions in the two hemispheres partly significant differences appear between certain conjugate locations. This is expected because the geomagnetic field distribution is not the same on both sides of the field line footprints. Still, we have to ensure current continuity. In order to check whether this is achieved by our approach to estimate the IHFAC intensity at E-region level, we averaged the current density over all latitudes and longitudes, separately for each MLT hour and for both hemispheres. As can be seen in Figure 5, the hourly mean curves from the two hemispheres track each other very well. This confirms the required current continuity between the two hemispheres.

### 3.2. Mean Features of the FMC

Next, we introduce the mean features of the derived meridional transverse currents that have never been shown before. Their characteristics are presented over the whole latitude range of  $\pm 50^\circ$  MLat. At low latitudes they are practically identical to the radial currents, IRC.

In the past there have been several studies devoted to IHFACs, but none has presented the meridional transverse current over the  $\pm 50^\circ$  MLat range. Figure 6 shows the MLT versus MLat distribution of averaged FMC at the different magnetic latitudes, separately for the four seasons. Overall, the current densities are smaller, reaching only one-third to one-half of those of the IHFAC. It has to be noted, however, that we are comparing here IHFACs at E-region level with local FMC at satellite altitude (460–410 km). The current intensity varies quite symmetrically between hemispheres. This is a consequence of our calculation procedure. When interpreting the mean value of the two FAC values at conjugate points as IHFAC, the remaining parts have then the same magnitude. The derived FMC values are thus a measure of the difference in FAC density derived at the two conjugate points, weighted by the local inclination angle. Positive values represent upward and poleward meridional currents, as shown in Figure 2.

Most prominent changes of FMC intensity are found for all seasons along the MLT axis. But there does not appear a clear diurnal variation. Furthermore, along the latitude axis, different characteristics can be identified

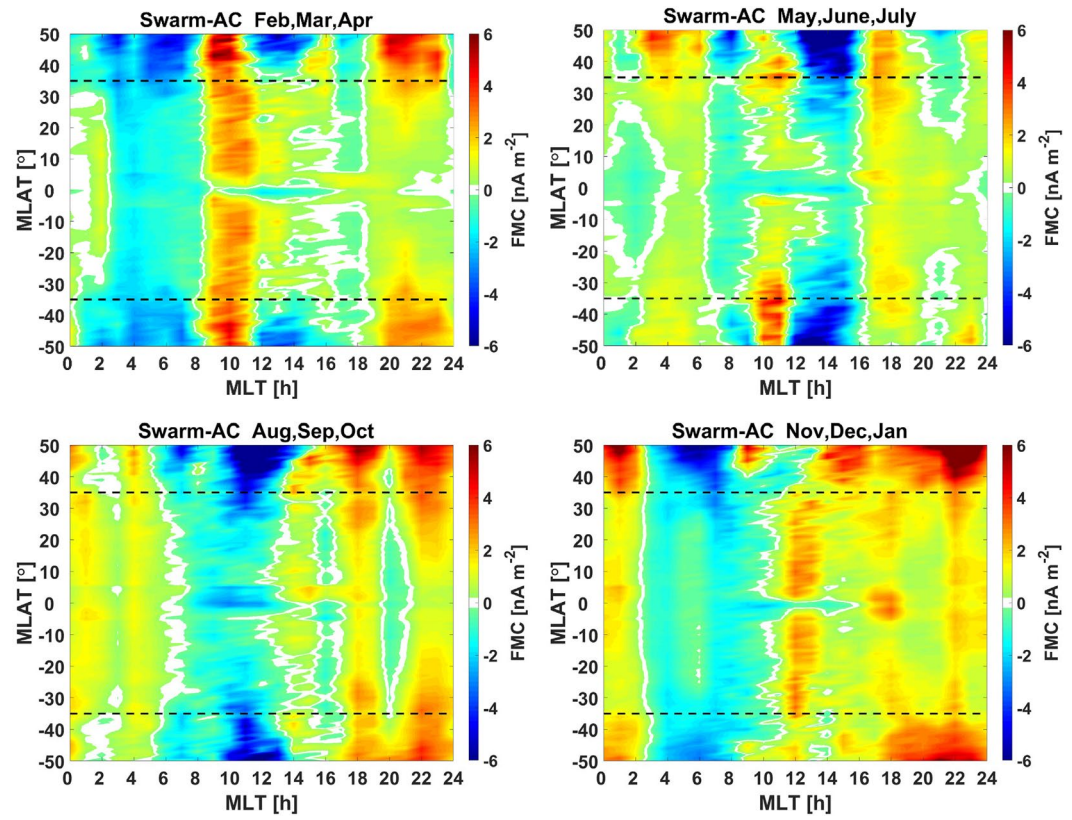


**Figure 6.** Magnetic latitude versus magnetic local time distributions of the FMC derived from Swarm A&C separately for four seasons (Feb–Apr, May–July, Aug–Oct, Nov–Jan).

between certain zones. We have added again the demarcation lines at  $\pm 35^\circ$  MLat at satellite altitude. At these borders also FMCs exhibit prominent changes. In most cases the intensity increases on the poleward sides. This means, here the differences between FAC intensities at conjugate points become larger. Common features present in all seasons are the narrow horizontal current strips right above the magnetic equator, within  $\pm 5^\circ$  MLat. These wind-driven F-region meridional current systems have been mentioned earlier in several studies, for example, Park et al. (2010), Lühr and Maus (2006), and Lühr et al. (2019). The current direction at satellite altitude is downward around noon and upward during evening hours. The recovery of this well-known current feature by these data provides confidence into our FMC estimation approach.

Next, we are also interested in the longitude distribution of FMC. For that purpose, the local time sectors around morning (06–07 MLT), noon (11–12 MLT), and evening (17–19 MLT) are considered. Figure 7 shows the FMC density in MLat versus geographic longitude (GLon) frames, separately for the four seasons, spring, summer, autumn, winter (Feb–Apr, May–Jul, Aug–Oct, Nov–Jan). Overall, the FMCs do not show so much longitude variation in any of the time sector. An outstanding feature appears between  $30^\circ\text{W}$  and  $60^\circ\text{W}$  GLon. This agrees well with the longitude sector of the SAA. Here the currents exhibit a more negative (downward) component in the morning and also in the evening sector (except for the December solstice). Conversely, around noon the currents are enhanced in outward direction at these longitudes. Again, December months make a difference. At present we cannot provide a good explanation for these particular FMC features in the SAA sector. However, it can be stated that the otherwise rather homogeneous longitudinal current distribution does not provide any sign of FMC tidal driving. It may also be questioned how far the dominating current intensities and directions, shown in Figure 7, reflect typical seasonal characteristics. From Figure 6 we know that these values can change strongly from hour to hour in any of the seasons. We thus have difficulties to deduce any typical FMC seasonal characteristics.

When looking at the latitude distribution in Figure 7 some common features can be found. Beyond  $\pm 35^\circ$  MLat the FMC is enhanced significantly at all longitude. At lower latitudes the distribution is rather homogeneous. Somewhat outstanding at all seasons is the narrow band above the magnetic equator. Here we find at all longitudes the

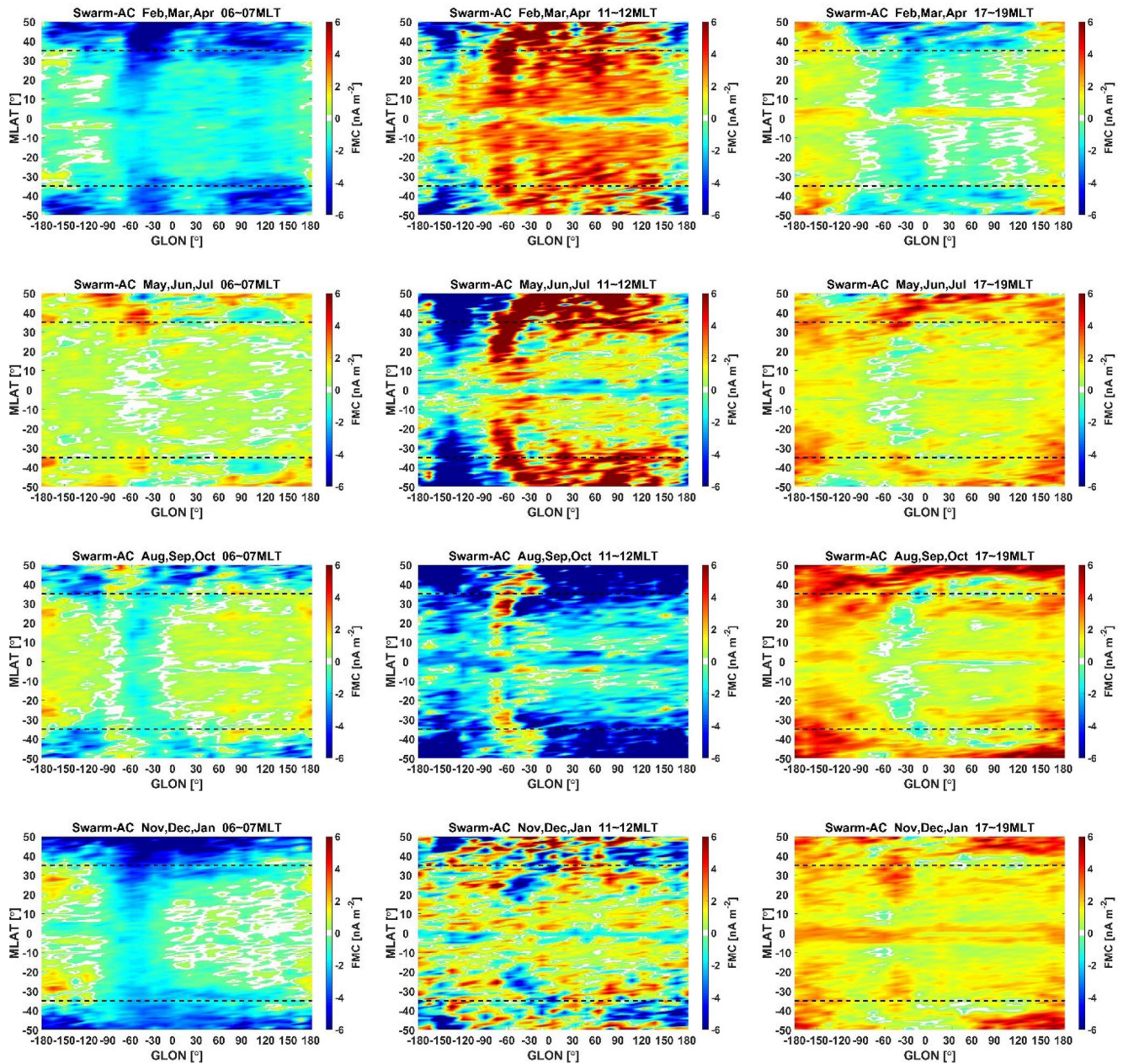


**Figure 7.** Magnetic latitude versus longitude distributions of the FMC derived from Swarm A&C around dawn, noon and dusk separately for four seasons (spring, summer, autumn, winter). FMC within  $\pm 5^\circ$  MLat is derived from IRC directly.

expected downward currents around noon and upward currents during evening hours. These features are caused, as mentioned above, by the wind-driven meridional F-region current system first predicted by Rishbeth (1971).

#### 4. Discussion

In this study we took great care to provide highly reliable estimates of the IHFAC for the first 5 years of the Swarm mission. Different from earlier studies, we have mapped the IHFACs down along the field line to the E-region, where they close, and we normalized the density value to the field strength at that reference altitude. This makes the results independent of satellite height and makes comparisons with other studies easier. Furthermore, for the first time, the mean transverse FMC is estimated for the same time interval. For this current component, the results are valid at the satellite position because there is no straight forward way of normalizing the current densities to a common altitude.

#### 4.1. IHFAC Characteristics

At the beginning we would like to discuss shortly the processes that cause IHFACs in the ionosphere. An instructive outline of the processes responsible for IHFACs has been given by Buchert (2020). He clearly stated that to first order field lines can be regarded as equipotential lines, thus there are no potential differences between the hemispheres. Rather, IHFACs reflect the difference in dynamo action between conjugate parts of the E-region. In the case of homogeneous conductivity distribution in the ionosphere the divergence of Pedersen currents,  $\nabla J_P$ , drives field-aligned currents. Here we have to distinguish between the locally generated  $J_P$  and the part of it driven by FACs. The presence of an IHFAC circuit requires that there is a hemispheric difference in the local generations, but the total  $J_P$ , including the part from FACs, has to be the same in both hemispheres, in order to satisfy the current continuity.

In a generator the current and the electric field,  $E$ , have opposite directions. The generated Pedersen current can thus be expressed as:

$$J_P = -\Sigma_P \cdot E \quad (8)$$

where  $\Sigma_P$  is height-integrated Pedersen conductivity. In a more general case also the effect of the neutral wind has to be considered.

$$J_P = -\Sigma_P(E - u \times B) \quad (9)$$

here  $u$  is the zonal neutral wind velocity and  $B$  the ambient magnetic field. It has to be noted that both  $E$  and  $u$  are frame-dependent. It may thus be more convenient to write the current generation equation in a somewhat different form:

$$J_P = \Sigma_P(v + u) \times B \quad (10)$$

where  $v$  is the plasma drift velocity at F-region altitude. Both  $u$  and  $v$  have to be taken in the same frame, for example, Earth-fixed, in which the B-field is constant. In the case of a generator plasma drift and wind velocity add up. In a load these two quantities are counter-streaming. Energy dissipation takes place in the hemisphere with the weaker generator.

When we are treating IHFACs, the associated Pedersen currents in both hemispheres have to be considered simultaneously. For the total  $J_P$ , which has to be the same in both hemispheres, we get:

$$J_P = \frac{\Sigma_{P,N}\Sigma_{P,S}}{\Sigma_{P,N} + \Sigma_{P,S}} \Delta[(v + u) \times B] \quad (11)$$

where  $\Sigma_{P,N}$  and  $\Sigma_{P,S}$  are the Pedersen conductances in the two hemispheres and the sign of  $\Delta[(v + u) \times B] = [(v + u) \times B]_N + [(v + u) \times B]_S$  determines the direction of  $J_P$  (positive northward). It has to be kept in mind that the B-field in the southern hemisphere comes with a negative sign. If we assume the  $\Sigma_{P,N} \gg \Sigma_{P,S}$ , Equation 11 can be simplified as:

$$\begin{aligned} J_P &= \frac{\Sigma_{P,N}\Sigma_{P,S}}{\Sigma_{P,N}} \Delta[(v + u) \times B] \\ &= \Sigma_{P,S} \Delta[(v + u) \times B] \end{aligned} \quad (12)$$

The intensity of  $J_P$  is thus mainly determined by the hemisphere with the smaller conductance. Strongest currents flow when both conductances are the same. Any hemispheric difference in  $u$ ,  $v$ , or  $B$  drives currents,  $J_P$  and IHFAC. Conversely, differences in conductances do not.

Most of the previous studies of IHFACs have focused on the low-latitude characteristics of the current distribution, for example, Yamashita and Iyemori (2002), Park et al. (2011), and Lühr et al. (2019). Just Park et al. (2020) noted the change in current characteristic at latitudes around 35° MLat. This significant change in IHFAC distribution and direction is well confirmed by the observations presented in our Figures 3 and 4. These figures may be compared with Figures 3d–3f and Figure 1 of Park et al. (2020), respectively. Although the main current features agree between the two works, there are subtle differences. Most obvious is the difference in current density. While Park et al. (2020) report in their Figures 1d–1f for noontime hours current densities up to 10 nA/m<sup>2</sup>, do we find for

this local time sector in Figure 4 peak current values up to 15 nA/m<sup>2</sup>. The difference in amplitude is even larger when comparing the mean diurnal variation of IHFACs for the summer period (see left panel of our Figure 3 and compare it with their Figure 3e). Here we find a factor of 3. Another obvious difference is the relative importance of IHFACs at low and mid latitude. From our Figure 3 a clear dominance of the IHFACs at low latitudes over the mid-latitude currents can be seen, while their Figure 3 suggests more prominent mid-latitude currents, which could facilitate a good part of current closure. This misleading impression is caused by their utilization of the radial current component, which gives the right current flow direction but fails to provide the correct intensity of field-aligned currents. As take-away message one may keep in mind that on average clearly stronger IHFACs flow at low than at mid latitudes.

#### 4.2. FMC Characteristics

The Swarm dual-SC Level 2 product “FAC” provides IRC as the prime result. This is primarily used for estimating the FAC distribution at middle and high latitudes. It is well known that there are also transverse currents in the meridional plane in the F-region. So far, the studies have focused on wind-driven meridional currents just above the magnetic equator. Here we try for the first time to derive F-region meridional currents at all low and mid latitudes. Main driver for these currents is thermospheric zonal wind. These winds exhibit characteristic diurnal and longitudinal patterns, that is, mainly westward from morning to afternoon and eastward in the evening and night (e.g., Liu et al., 2009). Our expectations had been that these characteristics can be found, at least partly, also in the FMC. Westward zonal winds drive downward (negative) meridional currents and eastward winds cause upward currents.

However, the derived mean FMCs (see Figure 6) show no clear diurnal variation following the wind patterns or the solar illumination state. Rather, current intensity and direction change partly from hour to hour in local time. It must be noted in this context that the Swarm satellites propagate only slowly through local times. For covering 1 hour it needs about 11 days, for ascending or descending node. If we find an outstanding feature for an hour, like the positive streak at 10 MLT in Figure 6 top left, that may reflect the special condition prevailing during the days it was sampled. During our 5-year period every local time hour is sampled about three times within a season. If the intensity and/or direction depend strongly on some environmental parameter, these three time samples may not be enough to reflect a true average. It may thus be worth to study in more details the variability of FMCs and their dependences from environmental conditions than investigating the mean values, which seem to be rather small.

Furthermore, we find no particular longitudinal patterns in the mean FMC distribution that would indicate any tidal modulation of the intensity. The only persistent longitudinal features appear in the sector of the SAA. Here upward currents are observed around noon and downward during morning and evening hours. Only months around December do not follow this scheme and show partly opposite deflections. We have presently no immediate explanation for the current structures in this confined longitude sector. Overall, it can be stated, the derived FMC is rather weak, compared to the IHFACs, and shows little systematic structure. It probably needs the support of numerical simulations to interpret the mean FMC distribution obtained in this study.

#### 4.3. Tidal Signatures of IHFAC

Since the early space-based studies of IHFACs, for example, by Park et al. (2011), it was noticed that their intensity is modulated by solar tides. During the summer and autumn seasons the prominent wave-4 longitudinal pattern has been reported for the low-latitude IHFAC part, for example, by Park et al. (2011) and Lühr et al. (2019). Differently in winter a wave-1 pattern dominates in this latitude range and is suggested to be related to the semidiurnal tidal component, SW1 (Lühr et al., 2019). But these authors also find an influence of the lunar tide M2 at this time of the year, in particular during years with stratospheric sudden warming events. These aforementioned tidal features are also found in the recent work by Wang et al. (2022) and in this study.

Different from that, tidal characteristics of the mid-latitude part of IHFAC have never been studied in some details. With the help of our advanced IHFAC estimates we have the chance to fill this gap. The typical approach is to look at latitudinal averages over a certain range of latitude. Figure 8 shows averages over 35°–50° MLat from both hemispheres plotted in frames of MLT over GLon. This is a suitable format for visualizing solar tidal activity. In the top row the observed variation of mean current density at mid latitudes is depicted separately

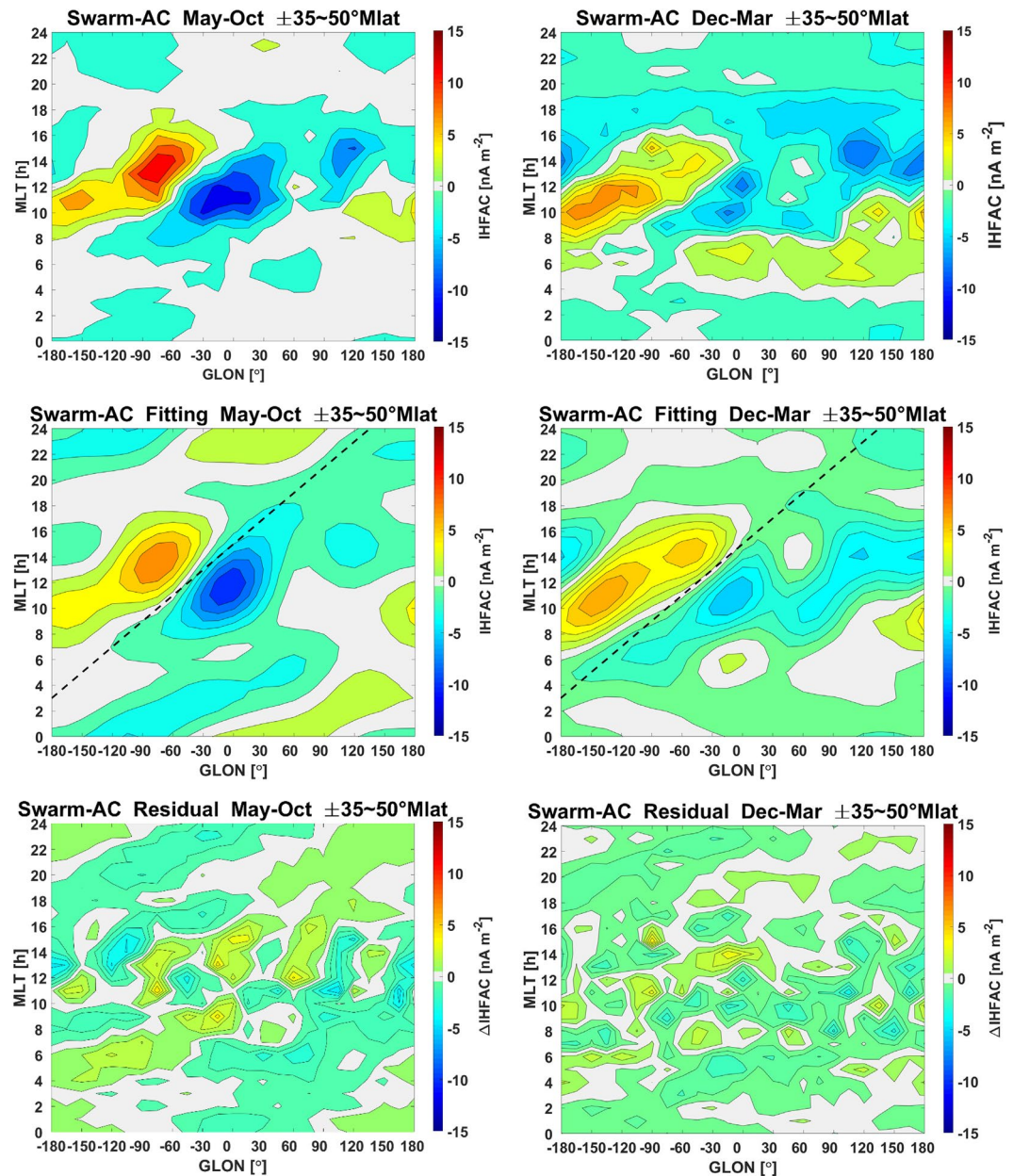


**Figure 8.** Magnetic local time versus geographic longitudinal distribution of IHFAC average over  $\pm 35^{\circ}$ – $50^{\circ}$  Mlat (top) observations (middle) synthetic signals and (bottom) residual during (left) summer and (right) winter seasons.

for our two periods. In order to remove the dominating diurnal variation averages over all longitudes have been subtracted hour by hour.

It is evident that intense IHFACs at middle latitudes are confined predominantly to daytime hours and the western hemisphere (including Europe). This statement is in principle true for both cases. We relate the localization of activity to tidal driving. In order to identify the relevant tidal components, which are mainly responsible for such longitudinal patterns, we fit a tidal model to the observations. In our study, we follow the method outlined in Häusler and Lühr (2009) and Xiong and Lühr (2013). For the determination of the tidal signatures, we first sort the current intensity into local time (1hr) versus longitude ( $15^{\circ}$ ) bins and remove the longitudinal mean values. These mean-free data are further processed by a Fourier transform which will bring forth the sum of observed tidal components for each wavenumber. In a last step, the dominant tidal components are used to reconstruct the synthetic current patterns in the LT versus longitude frame, which are compared with the observations. This step

**Table 1**  
*Tidal Spectrum Derived by Fitting a Tidal Model to the Observed IHFAC Distribution at Mid Latitudes*

IHFAC May–October			IHFAC December–March		
Component	Amplitude	Phase	Component	Amplitude	Phase
SP1	1.022	227.04	SP1	0.923	257.72
SP2	0.544	86.95	SP2	0.312	68.47
DE1	0.977	0.61	DE1	0.458	3.97
DE0	2.213	20.98	DE0	1.415	20.35
SE0	0.984	6.92	SE0	0.798	7.48
SW1	1.513	4.68	SW1	1.355	3.59
TW1	0.724	0.31	TW1	0.472	1.11
TW2	1.314	7.05	TW2	0.828	6.29

is used to confirm that the important tidal components have been considered. In the middle row of Figure 8 the derived tidal model is shown. For both periods a good fit with the observations is achieved. As proof for that the remaining residuals are depicted in the bottom row. Their values are nicely small and rather randomly distributed. This confirms a good representation of the tidal spectrum by the fitted model.

Table 1 lists the derived tidal components. A quite rich spectrum can be seen, but all these relevant tidal components contribute to the wave-1 and wave-2 longitudinal patterns. Due to the confinement of activity to daytime hours, higher harmonics are needed to reproduce the fading at night. This has earlier been shown in the context of EEJ and equatorial ionization anomaly (EIA) tidal features (e.g., Lühr & Manoj, 2013; Xiong & Lühr, 2013). The tide has probably a simpler spectrum. When looking at the amplitudes in Table 1, those contributing to wave-1 (SP1, DE0, SW1, TW2) are dominating in both periods. But also for the wave-2 components (SP2, DE1, SE0, TW1) appreciable amplitudes are found. It is just the superposition of these two wave patterns that causes the confinement of the main tidal activity to the western

hemisphere. Furthermore, there is a diagonal dashed lines added to the model fits of the tides (see Figure 8b). Any IHFAC activity appearing at a slope similar to that of the line occurs simultaneously in UT over the covered range of longitudes. Since major features in these plots are well aligned with the diagonal slope during daylight hours in the western hemisphere, the IHFAC activity variations at mid latitudes are obviously related to the effect of the SAA.

In order to have a closer look at that situation we plotted the synoptic IHFAC distribution in geographic latitude over GLon frames, separately for four selected UT times. Figure 9 presents in the left column the summer and in the right the winter IHFAC distributions. The top frames start with 18 UT, the most interesting one, and proceed to earlier times further down. The longitudes are always shifted that noon appears at the center. This set of frames give a quite different impression of the global IHFAC distribution. The qualitative differences between our two periods are much reduced, while the stronger currents in summer prevail. Also, the importance of the demarcation line at 37° MLat appears much reduced. Current structures at the two latitude bands complement each other rather well. The local time distribution is quite similar at the different longitudes, mainly northward IHFACs at low latitude during noontime, southward currents in the evening and also in the morning. For the latter we find an exception in the 18 UT case. Northward currents are prevailing in the middle Pacific region at that time.

An important finding from this study is the longitude (or UT) dependence of the overall IHFAC intensity. Figure 10 shows in the top row the mean global IHFAC density (adding up both northward and southward currents) for the different UT hours separately for our two periods. We find in both cases a clear maximum of total current between 16 and 18 UT. This coincides with the noon hours over the Americas. Interestingly, the total IHFAC curves for the two periods are very similar, but for summer the amplitudes are 10%–15% higher.

In the beginning of the discussion section, we had outlined the formulae that describe the intensity of IHFACs. Following Equation 11, the difference in magnetic field strength at conjugate points can have a great influence on the direction and intensity of IHFACs. Particularly prominent is the field difference in the longitude sector of the SAA (~20°W–70°W). Here the B-field is much depressed in the south. Thus, the field difference in the  $\Delta$ -term of Equation 11 provides a positive contribution. Around noontime westwards wind and plasma drifts are typically prevailing. That means, we obtain a negative value for  $J_p$  (southward current) in this local time sector. When comparing that with our observations, Figure 9 top row, we find for both periods around noon northward IHFACs at mid latitude and southward at low latitude. These have to be closed by southward  $J_p$  in both hemispheres, which fits well the predictions from the formulae. Nowhere else do we have a larger hemispheric difference in field strength than around the SAA, which agrees well with the peak in IHFAC intensity and direction at the time when noon passes over the SAA, see Figure 10.

The curves of the mean IHFAC density for our two seasons (Figure 10 top row) are very similar in shape. This may well be dominated by the hemispheric B-field differences, while neutral wind and plasma drift differences seem on average to be less important. The lower amplitudes during our winter strongly suggest a much-reduced mean conductance in the northern hemisphere. From our earlier discussion we know that the lower conductance

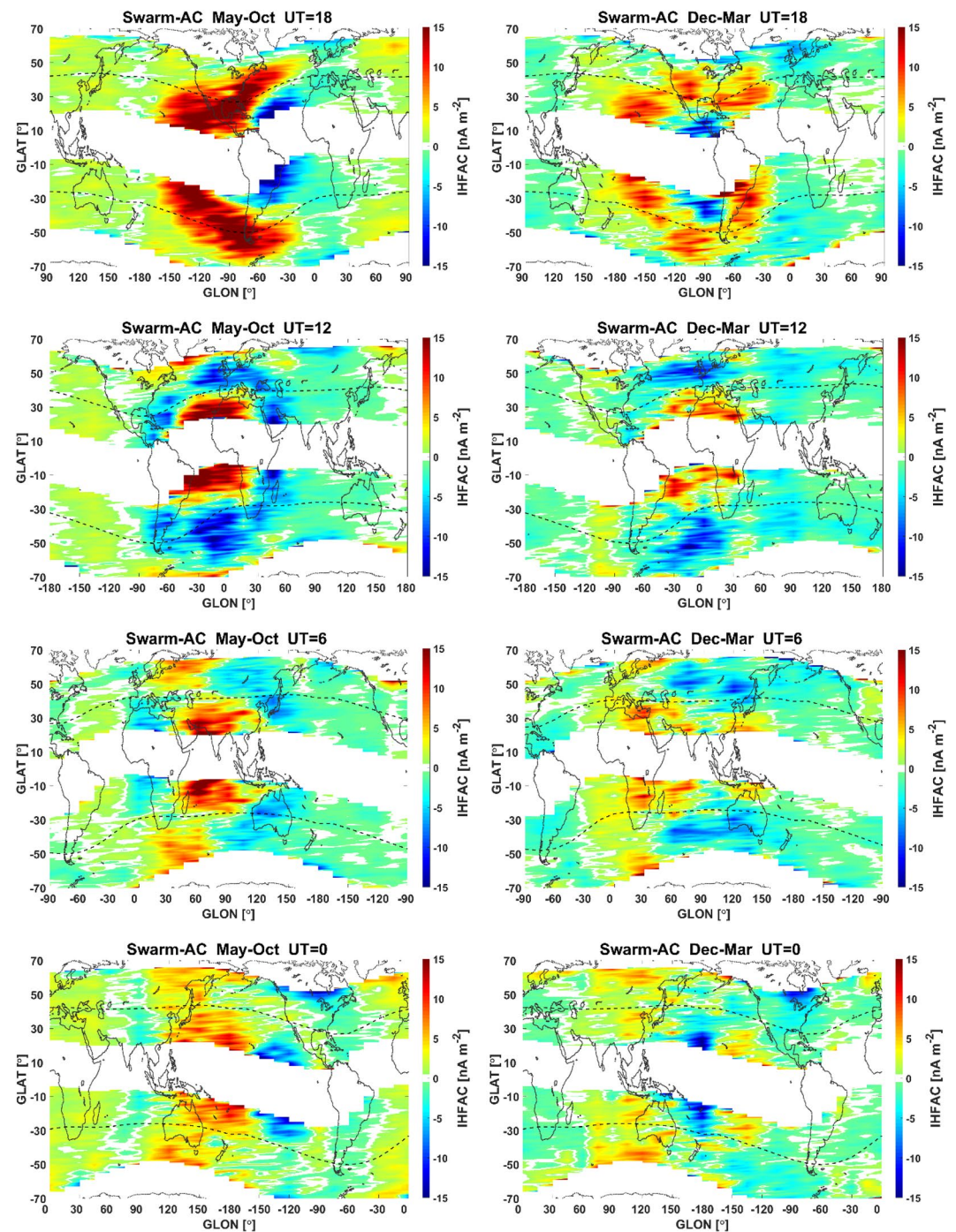


**Figure 9.** Geographic latitude versus longitude distribution of IHFAC from Swarm AC during (left) summer and (winter) winter season, separately for 00, 0600, 1200, and 1800UT. Blacked dashed lines denote  $\pm 37^\circ$  MLat.

determines the total current, and that strongest IHFACs are expected when the conductances in both hemispheres are equal. This fact indicates that hemispheric conductance differences are smaller during our summer than during our winter. The good northern hemisphere summer conductivity in this longitude sector ( $50^\circ\text{W}$ – $80^\circ\text{W}$ ) is obviously well matched by the generally enhanced conductance in the southern SAA region.

From the physical point of view all the IHFACs within a hemisphere should add up to zero, if there is no leakage to the high latitudes. This is required to fulfill the current continuity requirement. Figure 10 shows in the lower



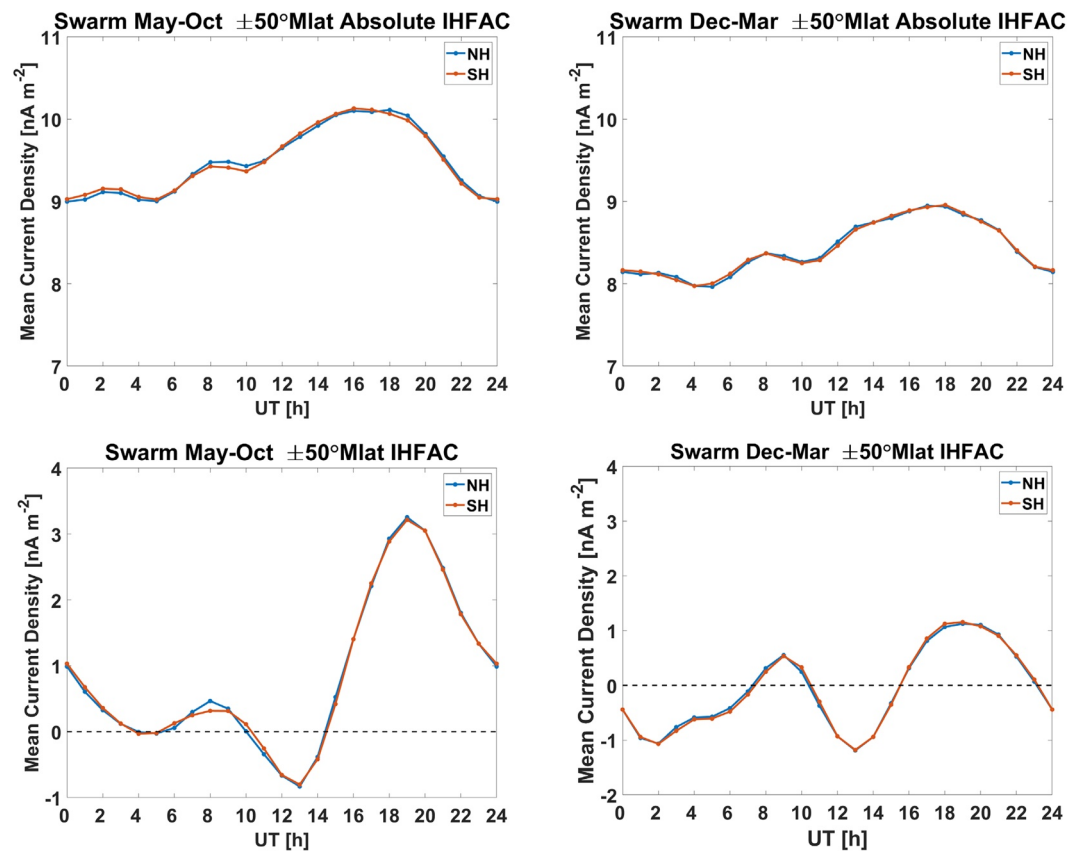


**Figure 10.** Global mean of absolute IHFAC current density values (top row) separately for each UT hour in both hemispheres for summer (left) and winter (right) periods (Bottom row) The same as above, but the mean IHFAC from signed current densities.

row the IHFACs from all bins of the global maps, as shown in Figure 9, added up separately for every UT hour and for the two periods. The obtained mean net currents are small but not zero. Also here, a northward directed net current is sticking out around 19 UT, in particular during summer. For explaining this apparent conflict, we have to remember that FAC estimates are only calculated for latitudes above  $\pm 15^\circ$  MLat. But from earlier studies, for example, Lühr et al. (2019), we know that IHFACs are present in Swarm IRC data down to  $\pm 5^\circ$  MLat. Their intensity, however, is difficult to quantify. Still, we argue that the missing current to balance the total IHFACs is probably flowing at the very low latitudes. A good indication for that can be found in the top row of Figure 9. At 18 UT we find intense northward IHFACs at middle latitudes. The expected return currents appear at low latitudes and most obviously, the main part is cut off by our limitation. The opposite situation prevails at 12 UT. Here, the northward current is cut off at low latitude around noon. Overall, we may state that our IHFAC estimates also satisfy the assumption of a globally closed IHFAC current system.

## 5. Summary

In this study we investigated the characteristics of IHFAC derived by the Swarm dual-satellite approach and by extending the analysis to middle latitudes. We have taken into account the varying ambient magnetic field intensities along the Swarm orbit and at the ionospheric E-region altitude for calculating the constant total IHFAC within a fluxtube connecting the two conjugate hemispheres. In addition, we have, for the first time, defined and evaluated the F-region meridional currents, FMC, over a wide latitude range. The main findings are summarized as:

1. The mean northward IHFAC density around noontime reduces remarkably poleward of  $\pm 37^\circ$  magnetic latitudes in summer and even reverse the direction during winter months. Even opposite flow directions of

- currents are found between low and mid latitudes within the 90°W–30°E longitude sector, occurring at noon and dusk during our two specifically defined seasons.
- For the first time the tidal signatures of IHFACs at middle latitudes are investigated. A superposition of the wave-1 (SP1, D0, SW1, TW2) and wave-2 (SP2, DE1, S0, TW1) patterns confine the tidal modulation of IHFACs in this latitude range to the dayside and to the western hemisphere in both periods. The tidal activity at middle latitudes is found to be better organized in UT than in MLT, with the strongest IHFAC appearing around 18–19 UT when noontime coincides with the American sector.
  - We relate the strongest IHFACs with their connection to the South Atlantic Anomaly, SAA. Here the hemispheric differences between the geomagnetic field strengths at conjugate points are particularly large, which is in favor of strong interhemispheric currents. The overall reduced IHFAC density during winter compared to our summer suggests an over-proportional reduction of northern hemisphere conductance compared to the southern during the months around December.
  - The mean F-region meridional currents, FMC, are highly symmetric with respect to the magnetic equator and quite weak, amounting only to about one-third or half of the IHFAC density. In addition, our FMC doesn't show characteristic longitudinal or diurnal variations, nor do they exhibit tidal wave signatures. More specific studies, possibly aided by numerical simulations, are needed to better disclose their typical features.

### Data Availability Statement

The authors want to thank the Swarm team for providing the data at ESA's website: <https://earth.esa.int/web/guest/swarm/data-access>.

### References

- Buchert, S. C. (2020). Entangled dynamos and Joule heating in the Earth's ionosphere. *Annales Geophysicae*, 38(5), 1019–1030. <https://doi.org/10.5194/angeo-38-1019-2020>
- Cain, J. C., & Sweeney, R. E. (1973). The POGO data. *Journal of Atmospheric and Terrestrial Physics*, 35(6), 1231–1247. [https://doi.org/10.1016/0021-9169\(73\)90021-4](https://doi.org/10.1016/0021-9169(73)90021-4)
- Campbell, W. H. (1989). The regular geomagnetic field variations during quiet solar conditions. In J. A. Jacobs (Ed.), *Geomagnetism* (Vol. 3, pp. 385–460). Academic Press.
- Fathy, A., Ghamry, E., & Arora, K. (2019). Mid and low-latitude ionospheric field-aligned currents derived from the Swarm satellite constellation and their variations with local time, longitude, and season. *Advances in Space Research*, 64(8), 0273–1177–1614. <https://doi.org/10.1016/j.asr.2019.07.022>
- Forbes, J. M. (1981). The equatorial electrojet. *Reviews of Geophysics*, 19(3), 469–504. <https://doi.org/10.1029/RG019i003p00469>
- Fukushima, N. (1976). Generalized theorem of no ground magnetic effect of vertical currents connected with Pedersen currents in the uniform conducting ionosphere. *Report of Ionosphere and Space Research in Japan*, 30, 35–40.
- Fukushima, N. (1979). Electric potential difference between conjugate points in middle latitudes caused by asymmetric dynamo in the ionosphere. *Journal of Geomagnetism and Geoelectricity*, 31(3), 401–409. <https://doi.org/10.5636/jgg.31.401>
- Häusler, K., & Lühr, H. (2009). Nonmigrating tidal signals in the upper thermospheric zonal wind at equatorial latitudes as observed by CHAMP. *Annales Geophysicae*, 27, 2643–2652. <https://doi.org/10.5194/angeo-27-2643-2009>
- Immel, T. J., England, S. L., Mende, S. B., Frey, H. U., Sagawa, E., Henderson, S. B., et al. (2006). Control of equatorial ionospheric morphology by atmospheric tides. *Geophysical Research Letters*, 33(15), L15108. <https://doi.org/10.1029/2006GL02616>
- Langel, R. A., Purucker, M., & Rajaram, M. (1993). The equatorial electrojet and associated currents as seen in Magsat data. *Journal of Atmospheric and Terrestrial Physics*, 55(9), 1233–1269. [https://doi.org/10.1016/0021-9169\(93\)90050-9](https://doi.org/10.1016/0021-9169(93)90050-9)
- Liu, H., Watanabe, S., & Kondo, T. (2009). Fast thermospheric wind jet at the Earth's dip equator. *Geophysical Research Letters*, 36(8), L08103. <https://doi.org/10.1029/2009GL037377>
- Lühr, H., Kervalishvili, G., Michaelis, I., Rauberg, J., Ritter, P., Park, J., et al. (2015). The inter-hemispheric and F-region dynamo currents revisited with the swarm constellation. *Geophysical Research Letters*, 42, 3069–3075. <https://doi.org/10.1002/2015GL063662>
- Lühr, H., Kervalishvili, G. N., Stolle, C., Rauberg, J., & Michaelis, I. (2019). Average characteristics of low-latitude interhemispheric and F region dynamo currents deduced from the swarm satellite constellation. *Journal of Geophysical Research: Space Physics*, 124(12), 10631–10644. <https://doi.org/10.1029/2019JA027419>
- Lühr, H., & Manoj, C. (2013). The complete spectrum of the equatorial electrojet related to solar tides: CHAMP observations. *Annales de Geophysique*, 31(8), 1315–1331. <https://doi.org/10.5194/angeo-31-1315-2013>
- Lühr, H., & Maus, S. (2006). Direct observation of the F region dynamo currents and the spatial structure of the EEJ by CHAMP. *Geophysical Research Letters*, 33(24), L24102. <https://doi.org/10.1029/2006GL028374>
- Lühr, H., Maus, S., & Rother, M. (2004). Noon-time equatorial electrojet: Its spatial features as determined by the CHAMP satellite. *Journal of Geophysical Research*, 109(A1), A01306. <https://doi.org/10.1029/2002JA009656>
- Lühr, H., Ritter, P., Kervalishvili, G., & Rauberg, J. (2020). *Applying the dual-spacecraft approach to the swarm constellation for deriving radial current density* (Vol. 17). Springer International Publishing. <https://doi.org/10.1007/978-3-030-26732-2>
- Onwumehili, C. A. (1992). A study of rocket measurements of ionospheric currents—III. Ionospheric currents at the magnetic dip equator. *Geophysical Journal International*, 108(2), 647–659. <https://doi.org/10.1111/j.1365-246X.1992.tb04644.x>
- Park, J., Lühr, H., & Min, K. W. (2011). Climatology of the inter-hemispheric field-aligned current system in the equatorial ionosphere as observed by CHAMP. *Annales Geophysicae*, 29(3), 573–582. <https://doi.org/10.5194/angeo-29-573-2011>

### Acknowledgments

This work is supported by the National Natural Science Foundation of China (42174191 and 42174186). Chao Xiong is supported by the Special Found of Hubei Luojia Laboratory (220100011) and the Dragon 5 cooperation 2020–2024 (project no. 59236).

- Park, J., Lühr, H., & Min, K. W. (2010). Characteristics of F-region dynamo currents deduced from CHAMP magnetic field measurements. *Journal of Geophysical Research*, *115*(A10), A10302. <https://doi.org/10.1029/2010JA015604>
- Park, J., Yamazaki, Y., & Lühr, H. (2020). Latitude dependence of interhemispheric field-aligned currents (IHFACs) as observed by the swarm constellation. *Journal of Geophysical Research: Space Physics*, *125*(2), 1–14. <https://doi.org/10.1029/2019JA027694>
- Rastogi, R. G. (1989). The equatorial electrojet. In J. Jacobs (Ed.), *Geomagnetism* (Vol. 3, pp. 461–525). Academic.
- Rishbeth, H. (1971). The F-layer dynamo. *Planet. Space Sciences*, *19*(2), 263–267. [https://doi.org/10.1016/0032-0633\(71\)90205-4](https://doi.org/10.1016/0032-0633(71)90205-4)
- Ritter, P., Lühr, H., & Rauberg, J. (2013). Determining field-aligned currents with the Swarm constellation mission. *Earth Planets and Space*, *65*(11), 1285–1294. <https://doi.org/10.5047/eps.2013.09.006>
- Van Sabben, D. (1964). North-south asymmetry of Sq. *Journal of Atmospheric and Terrestrial Physics*, *26*(12), 1187–1195. [https://doi.org/10.1016/0021-9169\(64\)90127-8](https://doi.org/10.1016/0021-9169(64)90127-8)
- Wang, F., Lühr, H., Xiong, C., & Zhou, Y. (2022). Improved field-aligned current and radial current estimates at low and middle latitudes deduced by the swarm dual-spacecraft. *Journal of Geophysical Research: Space Physics*, *127*(6), 1–16. <https://doi.org/10.1029/2022JA030396>
- Xiong, C., & Lühr, H. (2013). Nonmigrating tidal signatures in the magnitude and the inter-hemispheric asymmetry of the equatorial ionization anomaly. *Annales Geophysicae*, *31*(6), 1115–1130. <https://doi.org/10.5194/angeo-31-1115-2013>
- Xiong, C., Xu, J., Wu, K., & Yuan, W. (2018). Longitudinal thin structure of equatorial plasma depletions coincidentally observed by Swarm constellation and all-sky imager. *Journal of Geophysical Research: Space Physics*, *123*(2), 1593–1602. <https://doi.org/10.1002/2017JA025091>
- Yamashita, S., & Iyemori, T. (2002). Seasonal and local time dependences of the interhemispheric field-aligned currents deduced from the Orsted satellite and the ground geomagnetic observations. *Journal of Geophysical Research*, *107*(A11), 1372. <https://doi.org/10.1029/2002JA009414>